HTD-Vol. 182, Advances in Heat Exchanger Design,
Radiation, and Combustion
ASME 1991

ANALYSIS OF HEAT PIPE VAPOR DYNAMICS USING THE GALERKIN METHOD

F. Issacci, D. Huckaby, and I. Catton
Department of Mechanical, Aerospace and Nuclear Engineering
University of California
Los Angeles, California

ABSTRACT

The dynamic behavior of the vapor flow is analyzed for the heat pipes with axisymmetric geometry. The results show that the transient process involves multiple symmetric radial wave reflections about the symmetry line, as was observed in the two-dimensional analysis. Each wave reflection causes a significant increase in the local pressure and a large pressure drop along the heat pipe.

The cost of numerical studies of heat pipe dynamics is prohibitively expensive both in computational time used and in computer resource allocation. The potential of the Galerkin method is explored for the heat pipe analysis to significantly reduce the computational efforts.

Applying a Fourier analysis on the data resulted from the numerical calculations, it is shown that a few first terms of Fourier series, given the proper trial functions, will satisfactorily represent the data sets.

Nomenclature

A_{mn}	coefficients of series solution
b	heat pipe half width
B_{mn}	coefficients of series solution
C_m	beam function
c_p	specific heat
h_{fg}	latent heat of vaporization
k	thermal conductivity
L	heat pipe length
$\dot{m}$	mass flux
p	pressure
Q	input heat flux (W/m^2)
R	radial coordinate; dimensionless
r	radial coordinate
Re	Reynolds number
S_m	beam function
T	temperature
t	time
u	axial velocity
v	radial velocity
x	axial coordinate
X	axial coordinate; dimensionless
δ	liquid layer thickness
λ_m	eigenvalues of C_m
μ	viscosity
μ_m	eigenvalues of S_m
ρ	density
ρu	axial mass flux
ρv	vertical mass flux

Subscripts

a	adiabatic region
c	condenser
e	evaporator
eff	effective
0	initial value
sat	saturation

INTRODUCTION

This study is an extension of earlier work on the dynamics of the heat pipe vapor flow and the use of the Galerkin method in the heat pipe analysis (Issacci et al., 1991 and Issacci and Catton, 1991). The present study represents the transient analysis of the heat pipe vapor flow in cylindrical coordinates. The numerical results are then used to evaluate the potential of the Galerkin method to significantly reduce the required computational time.

A great deal of effort has gone into calculation of the behavior of the vapor phase of a heat pipe. Work by Bystrov and Goncharov (1983) led to the conclusion that a finite difference solution would be very costly. They found that the time step needed for stable advancement was on the order of 10^{-7} sec or smaller. This led them to a quasi-two-dimensional (2D) approach based on a simple cross-stream direction profile. Subsequent work by others such as Bowman (1987) came to similar conclusions. Bowman now calculates the vapor phase as a 1D process with influence coefficients (Bowman, 1990). As a result most heat pipe analyses assume 1D vapor flow, e.g. Bowman et al. (1990) and Chow and Zhong (1990). The one-dimensional assumption is a direct result of the cost of computation. The use of a 1D model of the vapor phase has, however, been shown to be questionable.

Experimental work by Galaktionov and Trukhanova (1985) shows that the temperature profile is not 1D even under steady state conditions. Experimental measurements by Marn et al. (1990) show that when a noncondensible gas is present, its concentration is 2D as is the temperature profile. This is in contradiction to the usual planar front approximation used in heat pipe analysis. The results of 2D transient and steady-state analyses by Tien and Rohani (1974), Faghri et al. (1989) and Jang et al. (1989) show that a 1D model of the vapor flow does not accurately predict the axial heat and mass transfer and pressure drop in a heat pipe. These are important considerations if the heat pipe is operated near its design limits.

The cost of two-dimensional numerical studies has been shown by Bystrov and Goncharov (1983), as mentioned above, Costello et al. (1986), Issacci et al. (1990) and Issacci et al. (1991) to be prohibitively expensive both in computer time used and in computer resource allocation. The computational time needed for calculation of a start-up process, is about two hours on CRAY 2, depending on the input heat flux and heat pipe geometry (Issacci et al., 1991). As a result of the expense associated with computation by numerical methods, one will not do very many. It is our view that a good system design needs to undergo a great deal of analytical scrutiny and this means one must develop good economical means for doing the analysis. The heat pipe is just one part of the system and its calculation should not be costly. This paper explores the feasibility of a method of efficient computation for the vapor phase of a heat pipe.

It is well known that the Galerkin method will be very efficient if the trial functions are appropriately selected. For example, a one-term approximation will yield fairly good results for flow in a rectangular duct. The Graetz problem yields good results for the first eigenvalue when a two term approximation is used. At the outset it was not clear how many terms would be needed to properly represent the vapor phase in a heat pipe.

The potential of the Galerkin method for heat pipe analysis was first explored by Issacci and Catton (1991). Using data sets from numerical calculations of a 2D heat pipe analysis (Issacci et al., 1991), they show that a few terms of a Fourier series would satisfactorily represent the data sets. They used trigonometric functions for the vertical direction and Beam functions for the axial direction.

Most of heat pipes in engineering applications have, however, an axisymmetric geometry. Therefore, the numerical code used in the previous work (Issacci et al., 1991) was improved to deal with axisymmetric coordinates. The numerical results are then used to demonstrate the feasibility of a Galerkin method by finding the proper trial functions for axisymmetric coordinates and showing that a few terms of a Fourier series will satisfactorily represent the data sets. A computer code using a Galerkin method then remains to be written.

It should be noted that our intent is not to develop a computer model of a heat pipe capable of dealing with shock structure. Shock structure is only of academic interest because the thermal capacity of the heat pipe walls softens transient behavior to the point that the vapor phase behaves almost in a quasi-static way. In other words a steady state model that properly includes certain multi-dimensional effects will be adequate for system analysis. As we will show, a few terms in a Galerkin approximation will be adequate for all but the fastest transients.

DESCRIBING EQUATIONS

A schematic of the vapor flow model used to represent the heat pipe is shown in Figure 1. The boundary of the vapor core is a thin porous medium which contains the working liquid. The input heat flux to the evaporator and the temperature of the outer surface of the condenser are specified. The planar side walls are assumed adiabatic.

The equations describing the vapor flow are the continuity, momentum, and energy equations, which are time dependent, viscous and compressible. An equation of state (EOS) is used to relate pressure to the density and temperature within the vapor core. These equations in axisymmetric coordinates (r,x) are

Continuity

$$\frac{\partial \rho}{\partial t}+\frac{\partial(\rho u)}{\partial x}+\frac{1}{r}\frac{\partial(r\rho v)}{\partial r}=0 \qquad (1)$$

x-Momentum

$$\frac{\partial(\rho u)}{\partial t}+\frac{\partial(\rho uu)}{\partial x}+\frac{1}{r}\frac{\partial(r\rho uv)}{\partial r}=-\frac{\partial p}{\partial x}+\frac{\partial}{\partial x}\left[\mu\frac{\partial u}{\partial x}\right]+\frac{1}{r}\frac{\partial}{\partial r}\left[\mu r\frac{\partial u}{\partial r}\right]+$$
$$\left\{\frac{\partial}{\partial x}\left[\mu\frac{\partial u}{\partial x}\right]+\frac{1}{r}\frac{\partial}{\partial r}\left[\mu r\frac{\partial v}{\partial x}\right]-\frac{2}{3}\frac{\partial}{\partial x}\left[\mu\frac{\partial u}{\partial x}+\frac{\partial rv}{\partial r}\right]\right\} \qquad (2)$$

r-Momentum

$$\frac{\partial(\rho v)}{\partial t}+\frac{\partial(\rho uv)}{\partial x}+\frac{1}{r}\frac{\partial(r\rho vv)}{\partial r}=-\frac{\partial p}{\partial r}+\frac{\partial}{\partial x}\left[\mu\frac{\partial v}{\partial x}\right]+\frac{1}{r}\frac{\partial}{\partial r}\left[\mu r\frac{\partial v}{\partial r}\right]+$$
$$\left\{\frac{\partial}{\partial x}\left[\mu\frac{\partial u}{\partial r}\right]+\frac{1}{r}\frac{\partial}{\partial r}\left[\mu r\frac{\partial v}{\partial r}\right]-\frac{2\mu v}{r^2}\right\}-\left\{\frac{2}{3}\left[\mu-\frac{1}{r}\frac{\partial}{\partial r}\mu r\right]\left[\frac{\partial u}{\partial x}+\frac{1}{r}\frac{\partial rv}{\partial r}\right]\right\} \qquad (3)$$

Energy

$$c_p\left[\frac{\partial(\rho T)}{\partial t}+\frac{\partial(\rho uT)}{\partial x}+\frac{1}{r}\frac{\partial(r\rho vT)}{\partial r}\right]=\frac{\partial p}{\partial t}+u\frac{\partial p}{\partial x}+v\frac{\partial p}{\partial r}+\frac{\partial}{\partial x}\left[k\frac{\partial T}{\partial x}\right]+$$
$$\frac{1}{r}\frac{\partial}{\partial r}\left[rk\frac{\partial T}{\partial r}\right]+\mu\left\{2\left[\frac{\partial u}{\partial x}\right]^2+2\left[\frac{\partial v}{\partial r}\right]^2+2\left[\frac{v}{r}\right]^2+\left[\frac{\partial u}{\partial r}+\frac{\partial v}{\partial x}\right]^2\right\} \qquad (4)$$

State

$$p=f(\rho,T) \qquad (5)$$

Initial and Boundary Conditions

The working liquid is assumed initially to be at a low temperature (close to the freezing point). Further, there is no input heat and the stagnant vapor is in thermodynamic equilibrium with the liquid. The boundaries of the vapor core are shown in Fig. 1. A no-slip, impermeable condition for the velocity and an adiabatic condition for the temperature are assumed on the side walls,

$$u=0, \qquad v=0, \qquad \partial T/\partial x=0 \qquad @ \quad x=0, L \qquad (6)$$

On the center line, the symmetry condition requires,

$$\partial u/\partial r=0, \qquad v=0, \qquad \partial T/\partial r=0 \qquad @ \quad r=0 \qquad (7)$$

In order to assign boundary conditions at the liquid-vapor interface, the liquid flow is assumed to be in a porous medium of thickness δ which is much smaller than the vapor core diameter. The axial velocity is assumed zero on this boundary,

$$u=0 \qquad @ \quad r=R_o \qquad (8)$$

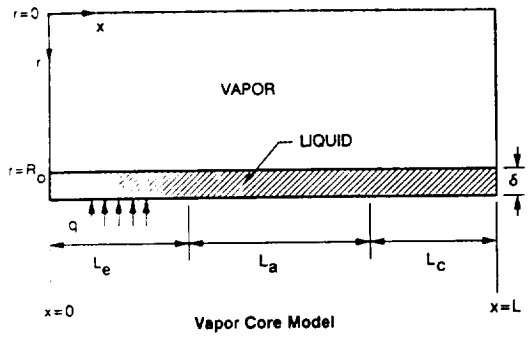

Figure 1. Vapor flow model in a heat pipe

To assign boundary conditions for the temperature and vertical velocity, the liquid-vapor interface is divided into three regions. In the evaporator zone the input heat flux, Q, is a given parameter and the input flow is approximated at $r = R_0$ and $0 \le x \le L_e$ by

$$\rho v = \dot{m} \simeq Q / h_{fg}(T), \qquad T = T_{sat}(p) \tag{9}$$

where h_{fg} is the heat of vaporization and $\dot{m}$ is the input mass flux. In the adiabatic zone, the boundary conditions are

$$v = 0, \qquad \partial T/\partial r = 0 \qquad @ \quad r = R_0, \quad L_e < x \le (L_e+L_a) \tag{10}$$

In the condensation zone the temperature T_c at the outer surface is given. By equating the heat of evaporation to the heat conduction in the liquid layer, the mass flux to the wall is approximated, at $r = R_0$ and $(L_e+L_a) < x \le L$, by

$$\rho v = \dot{m} \simeq -\frac{k_{eff}}{\delta}\left[\frac{T - T_c}{h_{fg}(T)}\right] \qquad T = T_{sat}(p) \tag{11}$$

where k_{eff} is the effective conductivity of the liquid layer and the temperature is assumed to be the saturation temperature corresponding to the pressure at the interface.

SOLUTION METHOD.

The five equations (1)-(5), with the initial and boundary conditions given by equations (6)-(11), have been numerically solved for the five variables ρ, ρu, ρv, T, and p using a real time computational procedure with a step change in wall heat flux at time t = 0. A finite-difference method has been used. The governing equations are highly nonlinear. For high-input heat flux, a high gradient velocity profile is created in the evaporator during the initial stages of the problem. Therefore, a shock capturing scheme is needed to accurately calculate the vapor flow variables. The solution method for the transient behavior of the vapor flow is described in Issacci et al. (1991). It was shown that a nonlinear filtering technique could successfully capture the shock-like velocity profiles. In an actual heat pipe, a step change in input heat flux to the vapor core is not expected. The shock like behavior dealt with by the numerical procedure will not be necessary.

FOURIER ANALYSIS

The Galerkin method used here represented by a Fourier analysis of the dependent parameters of the problem. One assumes an approximation for the parameter of interest,

$$\tilde{\rho u} = \sum_{m=1}^{M}\sum_{n=1}^{N} A_{mn}\, f_m(x)\, g_n(r) \tag{12}$$

substitutes into the governing equation

$$L(\tilde{\rho u}) = \varepsilon \tag{13}$$

then weights and integrates and sets the error ε to zero,

$$\int_x\int_r L(\tilde{\rho u})\, f_m(x) g_n(r) dx\, dr = 0, \quad m = 1,...,M \quad n = 1,...,N \tag{14}$$

to obtain an equation(s) for the coefficients A_{mn}.

For multi-dimensional compressible flows, this approach requires a great deal of tedious algebra. Before setting out to do this, we decided that the efficacy of the method should be tested. This was first done by Issacci and Catton (1991) using data sets from the numerical calculations of a 2D heat pipe analysis. Here, the numerical results of the analysis for the axisymmetric coordinates are used to find the proper trial functions and determine how many terms would be needed in the approximation.

The functions chosen to represent the problem parameters must satisfy the proper boundary conditions. It is particularly helpful, although not necessary, to choose orthogonal functions. A series solution for the axial mass flux, ρu, that has the proper symmetry and satisfies the proper boundary conditions is

$$\rho u(x,r,t) = \sum_{m,n} A_{mn}(t)\, C_m\!\left(\lambda_m \frac{x - L/2}{L}\right) J_0(\gamma_n r/R_0) + \sum_{m,n} A'_{mn}(t)\, S_m\!\left(\mu_m \frac{x - L/2}{L}\right) J_0(\gamma_n r/R_0) \tag{15}$$

The vertical mass flux, ρv, must be selected so that in the steady state limit

$$\frac{1}{r}\frac{\partial \rho r v}{\partial r} = -\frac{\partial \rho u}{\partial x} \tag{16}$$

as well as satisfy appropriate boundary conditions. A series representation that does this is

$$\rho v(x,r,t) = \sum_{m,n} B_{mn}(t)\, C'_m\!\left(\lambda_m \frac{x - L/2}{L}\right) J_1(\beta_n r/R_0) + \sum_{m,n} B'_{mn}(t)\, S'_m\!\left(\mu_m \frac{x - L/2}{L}\right) J_1(\beta_n r/R_0) \tag{17}$$

Scaling x and r,

$$R = r/R_0 \quad \text{and} \quad X = x/L - 1/2 \tag{18}$$

yields

$$\rho u(X,R,t) = \sum_{m,n} A_{mn}(t)\, C_m(\lambda_m X)\, J_0(\gamma_n R) + \sum_{m,n} A'_{mn}(t)\, S_m(\mu_m X)\, J_0(\gamma_n R) \tag{19}$$

$$\rho v(X,R,t) = \sum_{m,n} B_{mn}(t)\, C'_m(\lambda_m X)\, J_1(\beta_n R) + \sum_{m,n} B'_{mn}(t)\, S'_m(\mu_m X)\, J_1(\beta_n R) \tag{20}$$

The functions C_m and S_m and their first derivatives C'_m and S'_m, which are used for expansion in the x-direction, are orthogonal and vanish together with their first derivatives at the end-points, x = 0 and L. Such functions prove to be particularly useful in obtaining approximate solutions of the higher-order differential equations which arise in problems of hydrodynamics and hydromagnetic stability (Chandrasekhar, 1961). These functions are defined as

$$C_m(\lambda_m X) = \frac{\cosh \lambda_m X}{\cosh \lambda_m/2} - \frac{\cos \lambda_m X}{\cos \lambda_m/2} \tag{21}$$

$$S_m(\mu_m X) = \frac{\sinh \mu_m X}{\sinh \mu_m/2} - \frac{\sin \mu_m X}{\sin \mu_m/2} \tag{22}$$

$$C'_m(\lambda_m X) / \lambda_m = \frac{\sinh \lambda_m X}{\cosh \lambda_m/2} + \frac{\sin \lambda_m X}{\cos \lambda_m/2} \tag{23}$$

$$S'_m(\mu_m X) / \mu_m = \frac{\cosh \mu_m X}{\sinh \mu_m/2} - \frac{\cos \mu_m X}{\sin \mu_m/2} \tag{24}$$

where λ_m and μ_m (m = 1, 2, 3, ...) are the positive roots of the equations

$$\tanh \lambda_m/2 + \tan \lambda_m/2 = 0 \tag{25}$$

$$\coth \mu_m/2 - \cot \mu_m/2 = 0 \tag{26}$$

The orthogonality properties of the normalized functions C_m and S_m are

$$\int_{-1/2}^{1/2} C_m(\lambda_m X)\, C_n(\lambda_n X)\, dX = \delta_{mn}$$

$$\int_{-1/2}^{1/2} S_m(\mu_m X)\, S_n(\mu_n X)\, dX = \delta_{mn} \tag{27}$$

where δ_{mn} is the Dirac delta function, and

$$\int_{-1/2}^{1/2} C_m(X)\, S_n(X)\, dX = 0 \tag{28}$$

The first four roots of equations (25) and (26) are presented in Table I. For m > 4 the roots are found from

$$\lambda_m = (2m - 1/2)\,\pi \;\; ; \;\; \mu_m = (2m + 1/2)\,\pi \tag{29}$$

The functions C_m and S_m and their first three derivatives for m = 1, ..., 4 are tabulated by Harris and Reid (1958). Reid and Harris (1958) have also provided a useful sets of integrals involving the C- and the S-functions.

In equations (15) and (17), J_0 and J_1 are Bessel functions of zero and first order. γ_n and β_n are the eigenvalues of these functions, respectively, and are tabulated in Table II.

The coefficients in the series representations are found by Fourier analysis of the numerical data obtained from the transient analysis explained above,

$$A_{mn} = \int_{-1/2}^{1/2}\int_{0}^{1} R(\rho u) C_m(\lambda_m X) J_0(\gamma_n R/2)\, dR\, dX \tag{30}$$

$$A'_{mn} = \int_{-1/2}^{1/2}\int_{0}^{1} R(\rho u) S_m(\mu_m X) J_0(\gamma_n R/2)\, dR\, dX \tag{31}$$

$$B_{mn} = \int_{-1/2}^{1/2}\int_{0}^{1} R(\rho v) C'_m(\lambda_m X) J_1(\gamma_n R/2)\, dR\, dX \tag{32}$$

$$B'_{mn} = \int_{-1/2}^{1/2}\int_{0}^{1} R(\rho v) S'_m(\mu_m X) J_1(\gamma_n R/2)\, dR\, dX \tag{33}$$

RESULTS AND DISCUSSIONS

For the results shown in this section, the working fluid is liquid sodium at, initially, $p_0 = 10^3$ N/m^2 and $T_0 = 800$K. The geometric dimensions are $R_0 = 5$ cm, $L_e = L_a = L_c = R_0$. The results shown in the following sections are for the transient flow patterns in the vapor core and the Fourier analysis of these results.

Flow Patterns

Figure 2 shows the flow patterns in the vapor core for a high-input heat flux, $Q = 10^6$ W/m^2. The Reynolds number based on the vapor core diameter is Re = 200 and the computations were done for an optimized grid of 41 × 121. The optimized computational grid was chosen by inspection of the calculated L^2-error (see Issacci et al., 1990). The transient development of the radial mass flux ρv at different times is shown (Fig. 2). At t = 0, the vapor is stagnant. Evaporation takes place as the input heat flux is applied. Since the input heat flux is high, a shock-like wave is created (Fig. 2a). The vapor flow develops above the evaporator and in the adiabatic region and the wave travels above the evaporator until it hits the center line (Fig. 2b) where the radial mass flow is blocked, ρv = 0. At this point, the vapor is compressed and the vapor pressure increases which causes a negative radial pressure gradient and the wave reflects back (Fig. 2c). The figure also shows reverse flow in the bottom left corner which is caused by wave reflection. When the reflected wave reaches the upper boundary (Fig. 2d) and the vapor is

Table I. The First Four Eigenvalues of the Beam Functions

m	λ_m	μ_m
1	4.730040	7.853204
2	10.995607	14.137165
3	17.278759	20.420352
4	23.561944	26.703537

Table II. The First Six Eigenvalues of the Bessel's Functions

n	γ_n	β_n
1	2.4048	1.84118
2	5.5201	5.33144
3	8.6537	8.53632
4	11.7915	11.70600
5	14.9309	14.86359
6	18.0711	18.01553

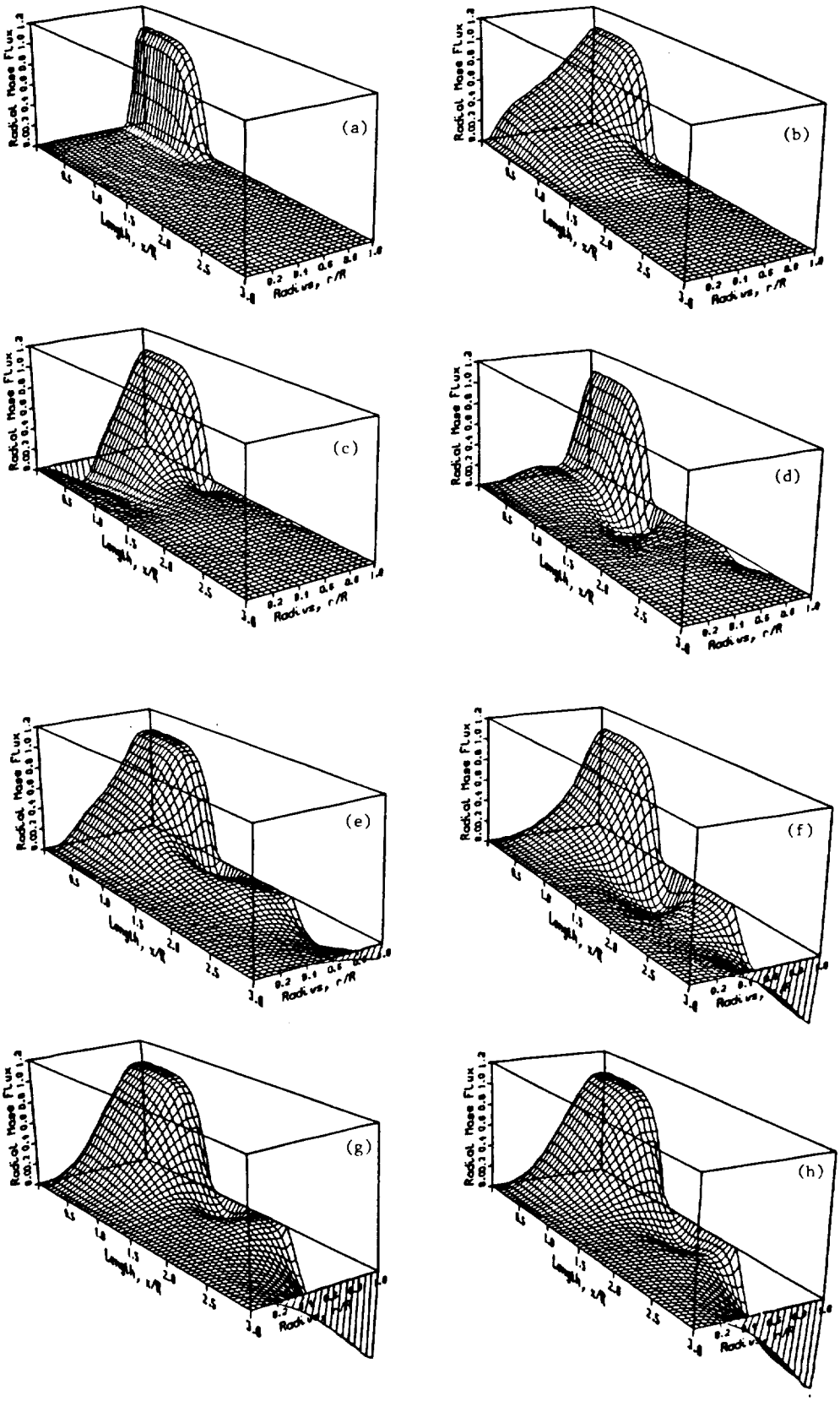

Figure 2. Transient development of the radial mass flux

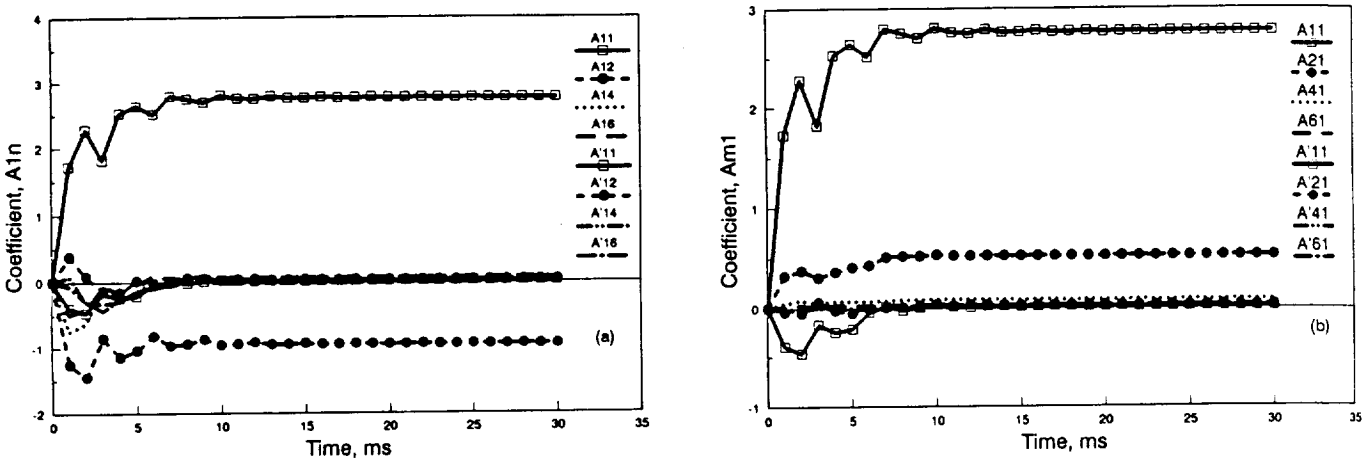

Figure 3. Coefficients A_{1n} and A_{m1} for different n and m

compressed within the evaporation region, the radial pressure gradient is reduced and the inflow mass flux tries again to fill the evaporation region (Fig. 2e). As the vapor fills the evaporation region, another wave reflection occurs. Each reflection of the shock-like wave causes a significant increase in the local pressure and, consequently, a large pressure drop along the heat pipe.

The wave reflections in the evaporation region also affect the flow pattern in the adiabatic region. Figure 2d shows that when the reflected wave reaches the upper boundary of the evaporator, circulation is initiated in the adiabatic region. Figures 2f and 2g demonstrate the subsequent set of reflection and refill of the vapor flow. When the process reaches steady-state conditions, circulation in the adiabatic region occupies a significant portion of the region.

The transient flow pattern in the condensation region is also illustrated in Fig. 2. At early stages of the transient process, the vapor is at the same temperature as the liquid and, as a result, there is no condensation (no outflow, Figs. 2a and 2b). When vapor at higher temperatures flows from the evaporator to the condensation region, the vapor temperature in the condenser increases. A temperature gradient is thus established along the liquid layer and condensation takes place (Fig. 2d). The vapor temperature in the condenser increases with time and, consequently, the condensation rate increases. At steady state, shown in Fig. 2h, the mass flow through the evaporator equals the mass flow out of the condenser.

The same type of flow patterns and wave reflections was also observed in the transient analysis of heat pipe using Cartesian coordinates (Issacci et al., 1991). In that study, speculation was that for axisymmetric coordinates, wave reflections in the evaporation region and flow reversal in the adiabatic region would not occur. The present study shows, however, that this is not the case and for both geometries high-input heat flux will cause a pressure drop in the vapor that is significantly higher than that found for steady-state conditions.

Fourier Analysis of the Data

The results obtained from the above analysis were used to check the feasibility of using the Galerkin method in heat pipe analysis. The Galerkin method can be very effective if the first few coefficients are sufficient to represent the data. Figures 3(a) and 3(b) show the first coefficients of a representative calculation. In Figure 3(a) it is shown that the first two coefficients in the y-direction (index -n) are the dominant ones. The same is true for the coefficients in the x-direction (index -m) shown in Figure 3(b).

Figures 4 and 5 show the few first coefficients as functions of time for different input heat fluxes for axial and radial mass fluxes, respectively. The periodic oscillations of these coefficients with time is caused by the multiple wave reflections in the evaporator as shown in Fig. 2. Figures 4 and 5 imply that the mean behavior of the coefficients can be predicted by an exponential asymptote.

The presence of shock-like features in the solution, shown in Fig. 2, poses an extreme challenge to expansions in orthogonal functions, which lack the shock-capturing capability. Although once the shock dissipates the expansion coefficients exhibit a decent decay (Figs. 3 to 5), they decay slowly at the start. This implies that at early stages of the transient process, large number of terms in the expansions are needed to accurately represent the solution. Under these conditions, the Galerkin method could lose its advantages over the finite-difference method.

After a short time, Figs. 3 to 5 show significant decay in the oscillations. As a result, the number of terms in the expansions decreases significantly with time. Furthermore, in an actual heat pipe, the thermal capacity of the walls softens the transient behavior and a step change in the input heat flux to the vapor core is not expected. Under these conditions, the number of terms in the expansions are few and the Galerkin method can successfully be used in the heat pipe analysis.

One of the major conclusions of previous studies of the dynamic behavior of vapor flow in heat pipes is that, in the complete analysis of heat pipes, the vapor flow can be assumed quasi-steady state. This conclusion is based on the fact that the characteristic time of the vapor flow is significantly smaller than that of the liquid flow. Under assumption of quasi-steady state, the coefficients of the series solutions will only be functions of the input heat flux. Figure 5 shows dependency of the few first coefficients on the input heat flux at steady state. These figures suggest that the coefficients can be represented by a polynomial in terms of log Q, where Q is the input heat flux applied to the evaporator. A general formulation for this dependency is assumed as

$$\text{COEFF} = a_o + a_1 \log Q + a_2 (\log Q)^2 \qquad (34)$$

where COEFF denotes the coefficients A_{mn}, A'_{mn}, B_{mn} and B'_{mn}. The constants of the above equation for the first few coefficients are presented in Table III.

Figures 7(a) to 7(c) show the axial mass velocity profile under steady state condition at three different cross sections of the heat pipe; middle of the evaporator, adiabatic region and condenser, respectively. The data from the numerical analysis is shown by a solid curve. Series solutions with different number of terms are also shown. In all the figures, it is shown that the calculated data can be easily represented by the few first coefficients in the series solutions. The same conclusion can be drawn for the radial mass flux at the cross section $r = 0.25R_0$, shown in Figure 8.

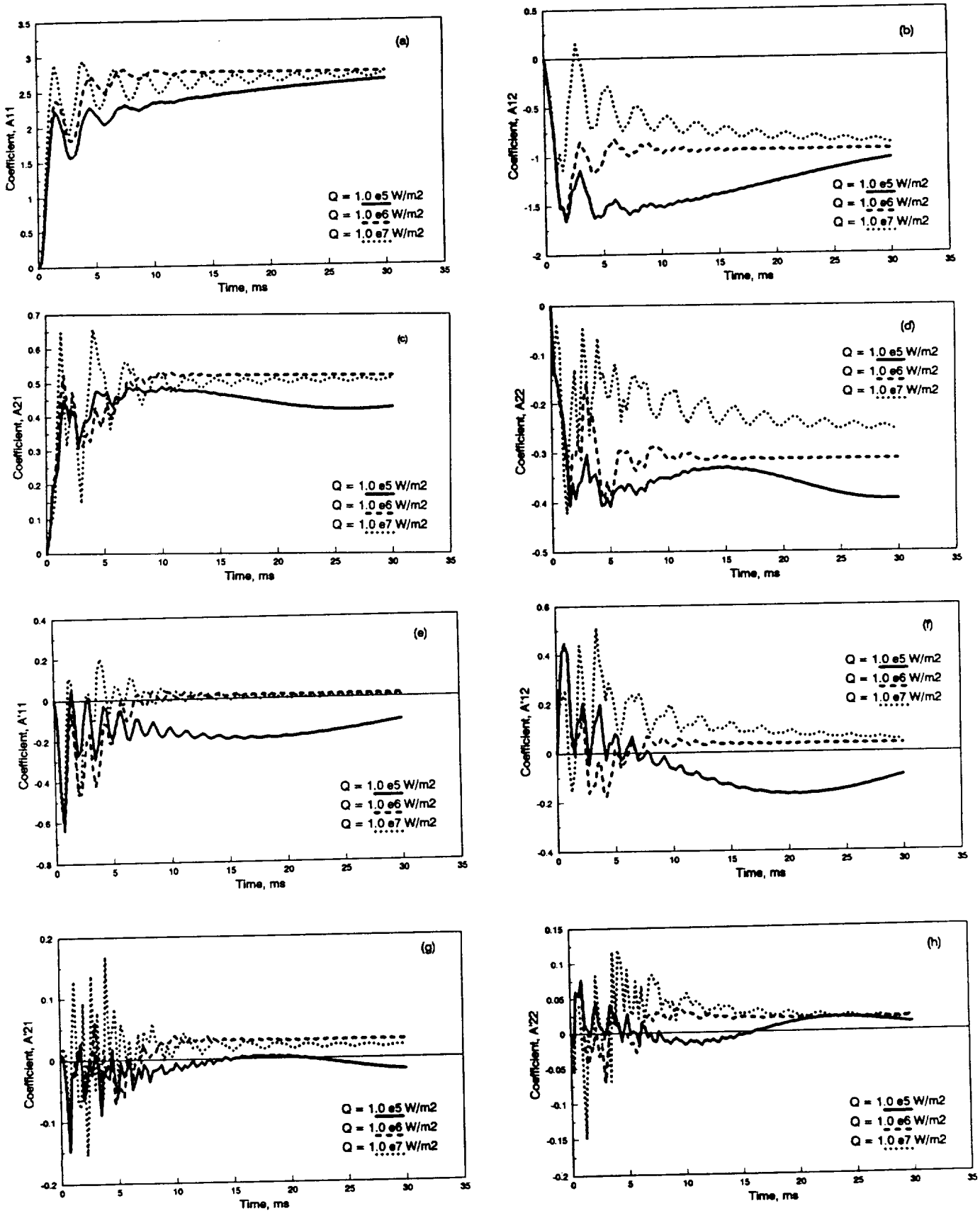

Figure 4. First coefficients for different input heat fluxes; axial mass flux

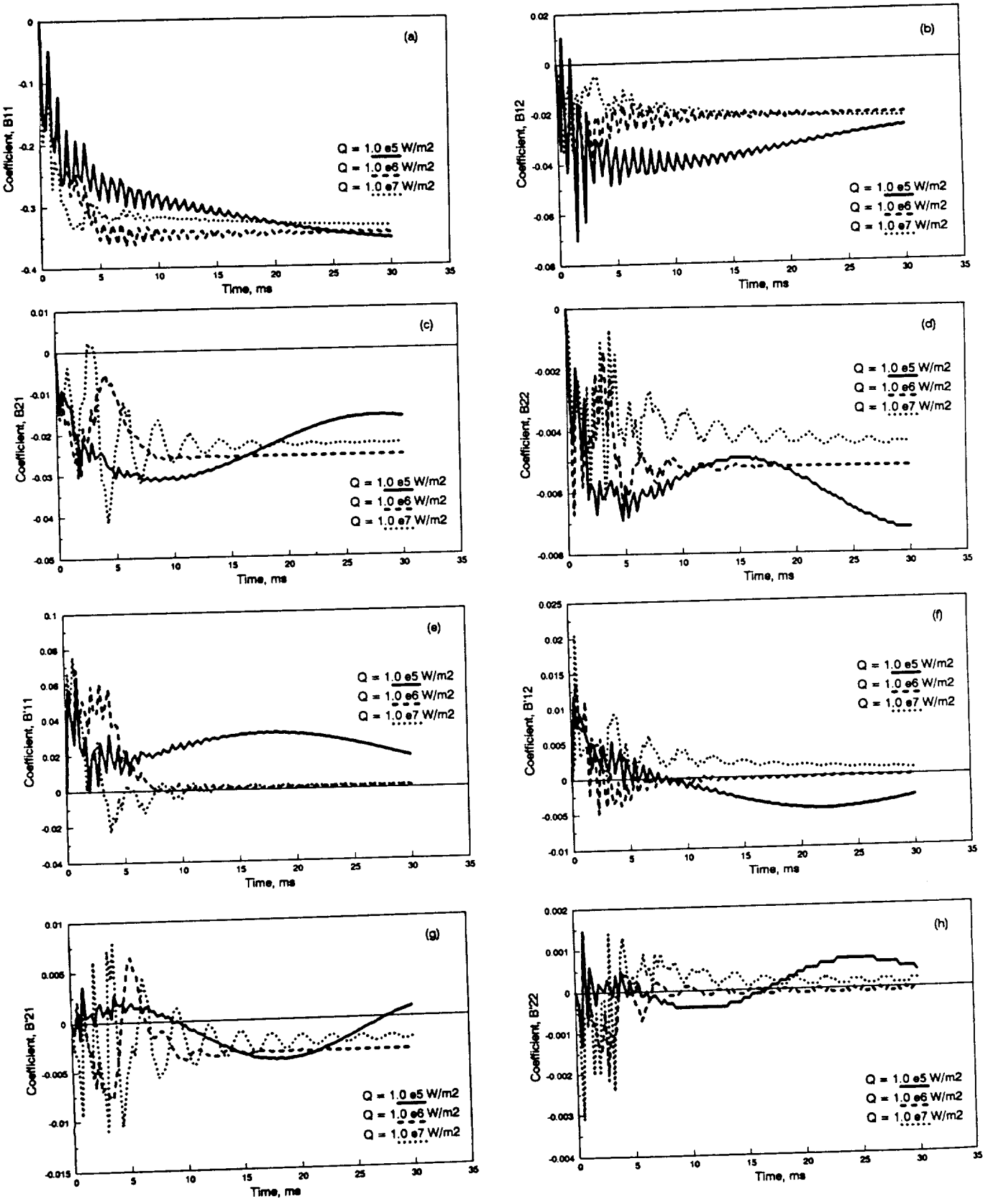

Figure 5. First coefficients for different input heat fluxes; radial mass flux

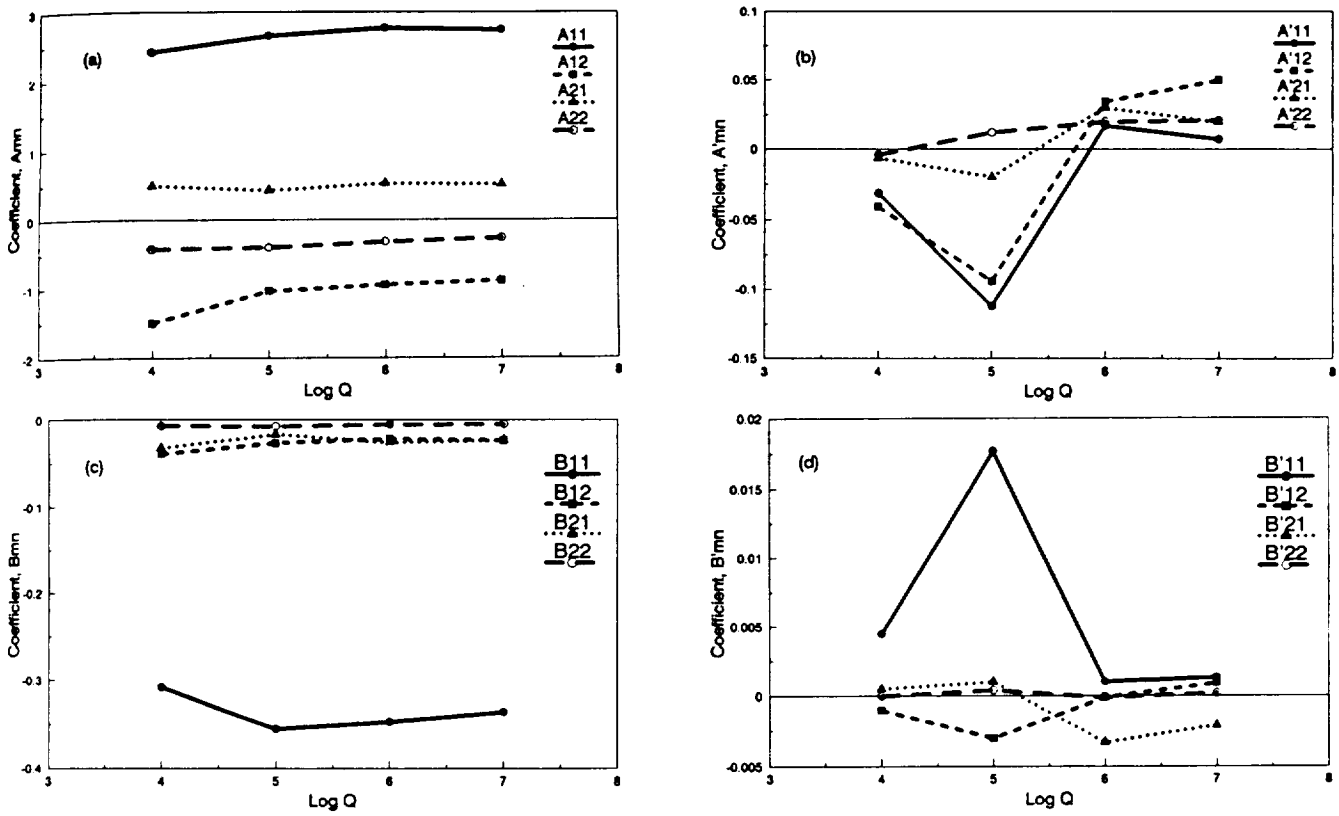

Figure 6. Coefficients as functions of input heat flux

For a steady state or quasi-steady state, a good approximation can be obtained for ρu using a five term approximation, see Figures 3 and 4. The result is

$$\rho u = A_{11}\, C_1(\lambda_1 X)\, J_0(\gamma_1 R) + A_{12}\, C_1(\lambda_1 X)\, J_0(\gamma_2 R) + A'_{11}\, S_1(\mu_1 X)\, J_0(\gamma_1 R) + A'_{12}\, S_1(\mu_1 X)\, J_0(\gamma_2 R) A_{21}\, C_2(\lambda_2 X)\, J_0(\gamma_1 R) + \quad (35)$$

Using the coefficients presented in Table III, ρu at steady state can be represented in terms of the input heat flux as

$$\begin{aligned}\rho u = {} & (0.16 + 0.82 \log Q)\, C_1\, (\lambda_1 X)\, J_0(\gamma_1 R) + \\ & (-5.08 + 1.31 \log Q)\, C_1\, (\lambda_1 X)\, J_0(\gamma_2 R) + \\ & (0.35 - 0.17 \log Q)\, S_1\, (\mu_1 X)\, J_0(\gamma_1 R) + \\ & (0.26 - 0.15 \log Q)\, S_1\, (\mu_1 X)\, J_0(\gamma_2 R) + \\ & (0.80 - 0.13 \log Q)\, C_2\, (\lambda_2 X)\, J_0(\gamma_1 R) \end{aligned} \quad (36)$$

where Q is in W/M^2. Similarly ρv at steady state can be represented by the following five-term approximation

$$\begin{aligned}\rho v = {} & (0.13 - 0.17 \log Q)\, C'_1\, (\lambda_1 X)\, J_1(\gamma_1 R) + \\ & (-0.15 + 0.04 \log Q)\, C'_1\, (\lambda_1 X)\, J_1(\gamma_2 R) + \\ & (-0.07 + 0.03 \log Q)\, S'_1\, (\mu_1 X)\, J_1(\gamma_1 R) + \\ & 0.016\, S'_1\, (\mu_1 X)\, J_1(\gamma_2 R) + \\ & (-0.13 + 0.04 \log Q)\, C'_2\, (\lambda_2 X)\, J_1(\gamma_1 R) \end{aligned} \quad (37)$$

Table III. The Constants in Equation 34

COEFF	a_0	a_1	a_2
A_{11}	0.1572	0.8237	-0.0648
A_{12}	-5.0850	1.3067	-0.1012
A_{21}	0.8018	-0.1357	0.01383
A_{22}	-0.4027	-0.03903	0.008650
A'_{11}	0.3506	-0.1708	0.01775
A'_{12}	0.2658	-0.1492	0.01720
A'_{21}	-0.0402	0.00384	0.000800
A'_{22}	-0.1440	0.05030	-0.003825
B_{11}	0.1297	-0.1686	0.01465
B_{12}	-0.1562	0.04315	-0.00345
B_{21}	-0.1291	0.03765	-0.00325
B_{22}	-0.0055	-0.001220	0.000200
B'_{11}	-0.0729	0.03284	-0.003225
B'_{12}	0.0162	-0.007390	0.0007500
B'_{21}	0.01075	-0.003135	0.0001750
B'_{22}	-0.000655	0.000285	-0.000025

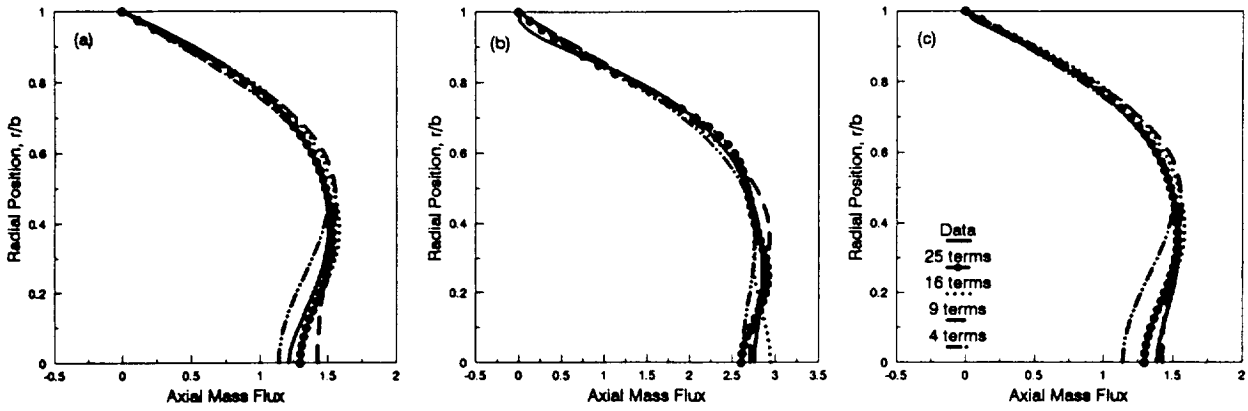

Figure 7. Series solutions compared to the calculated axial mass flux at the middle of (a) evaporator, (b) adiabatic region, (c) condenser

When the quasi-steady approximation is valid, which we believe will most often be the case, one only needs substitute for the instantaneous value of Q (W/m^2) in the above equations. It is clear that this approach will yield fast economic results for the vapor phase of a heat pipe.

CONCLUSIONS

The dynamic behavior of the vapor flow is analyzed for the heat pipes with axisymmetric geometry. The results show that the transient process involves multiple symmetric radial wave reflections about the symmetry line, as was observed in the two-dimensional analysis. Each wave reflection causes a significant increase in the local pressure and a large pressure drop along the heat pipe.

The potential benefits from using the Galerkin method has also been studied for the heat pipe analysis. It has been shown that the numerical data for the mass flux in different directions can be represented in a series form. The most complicated mass flux profile under steady state condition is well represented by first few terms in the series. Interpolation allows one to deal with different heat fluxes.

For a given heat pipe, several numerical solutions can be used to obtain the coefficients in a Galerkin type representation. The Galerkin representation allows one to represent the dynamic behavior of the heat pipe for use in space thermal models at very little computational cost.

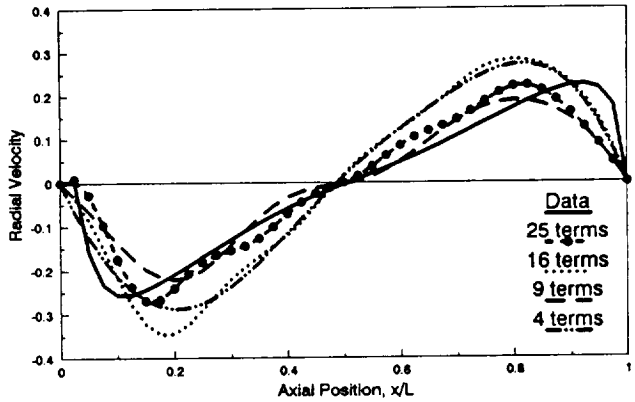

Figure 8. Calculated radial mass flux compared to the series solutions

ACKNOWLEDGEMENT

This work was supported by NASA Lewis under Contract No. NAG3-899 and NASA Dryden under Contract No. NCC2-374 Supp. 2.

REFERENCES

Bowman, W.J., 1987, "Simulated Heat Pipe Vapor Dynamics," *Ph.D. Dissertation*, Air Force Institute of Technology.

Bowman, W.J., 1990, NASA Workshop on Transient Heat Pipe Analysis.

Bowman, W.J., McClure, W.C., and Towne, M., 1990, "Transient Heat Pipe Modeling, Part 2," *AIAA 28th Aerospace Sciences Meeting*, Reno, Nevada, AIAA Paper No. 90-0061.

Bystrov, P.I., and Goncharov, V.F., 1983, "Starting Dynamics of High Temperature Gas-Filled Heat Pipes," *High Temperature*, Vol. 21, pp 927-936.

Chandrasekhar, S., 1961, *Hydrodynamic and Hydromagnetic Stability*, Dover, New York.

Chow, L., and Zhong, J., 1990, "Analysis of Heat Pipe Start-up from the Frozen State," *AIAA/ASME 5th Joint Thermophysics and Heat Transfer Conf.*, Seattle, WA.

Costello, F.A., Montague, A.F., and Merrigan, M.A., 1986, "Detailed Transient Model of a Liquid-Metal Heat Pipe," *Proc., AIAA/ASME 4th Joint Thermophysics and Heat Transfer Conf.*, Boston, MA.

Faghri, A., Chen, M-M., and Mahefkey, E.T., 1989, "Simultaneous Axial Conduction in the Fluid and the Pipe Wall for Forced Convective Laminar Flow with Blowing and Suction at the Wall," *Int. J. Heat Mass Transfer*, Vol. 32, No. 2, pp 281-288.

Galaktionov, V.V., and Trukhanova, L.P., 1985, "Study of the Process of Heat and Mass Transfer in the Region of the Vapor-Gas Front in a Gas-Regulated Heat Pipe," *J. Eng. Physics*, Vol 48, pp 296-300.

Harris, D.L., and Reid, W.H., 1958, "On Orthogonal Functions which Satisfy Four Boundary Conditions. I. Tables for Use in Fourier-Type Expansion," *Astrophys. J. Supp. Ser*, Vol. 3, pp 429-

Issacci, F., Ghoniem, N.M., and Catton, I., 1990, "Vapor Flow Patterns During Start-up Transient in Heat Pipes," *AIAA/ASME 5th Joint Thermophysics and Heat Transfer Conf.*, ASME, HTD-Vol. 135, pp 33-39, Seattle, WA.

Issacci, F., and Catton, I., 1991, "Use of Spectral Methods for Heat Pipe Analysis," 27th National Heat Transfer Conference, Minneapolis, Minnesota.

Issacci, F., Catton, I., and Ghoniem, N.M., 1991, "Vapor Dynamics of Heat Pipe Start-up," to appear in *J. Heat Transfer*.

Jang, J.H., Faghri, A., Chang, W.S., and Mahefkey, E.T., 1989, "Mathematical Modeling and Analysis of Heat Pipe Start-up from the Frozen State," *Heat Transfer with Phase Change*, ASME HTD-Vol. 114.

Marn, J., Issacci, F., and Catton, I., 1990, "Measurements of Temperature and Concentration Fields in a Rectangular Heat Pipe," *Heat Transfer in Space Systems*, ASME, HTD-Vol. 135, pp 33-39.

Reid, W.H., and Harris, D.L., 1958, "On Orthogonal Functions which Satisfy Four Boundary Conditions. II. Integrals for Use in Fourier-Type Expansion," *Astrophys. J. Supp. Ser*, Vol. 3, pp 448-452.

Tien, C.L., and Rohani, A.R., 1974, "Analysis of the Effects of Vapor Pressure Drop on Heat Pipe Performance," *Int. J. Heat Mass Transfer*, Vol. 17, pp 61-67.